that should predominantly contain three DNA polymerases (fig. S6 and supporting methods). No appreciable differences were observed in either the efficiency, or kinetics, with which replication was reinitiated downstream of the CPD.

We next analyzed the products of bulk and column-isolated, Eco RI–dependent CPD-template reactions by two-dimensional gel electrophoresis to establish if the restart products detected in denaturing gels were associated with the transition from stalled fork to full-length duplex DNA (Fig. 2, A and B). As seen for both reactions, the stalled fork was composed of the 5.3-kb stall product and a smear of Okazaki fragments. Restart fragments were exclusively associated with full-length duplex products, supporting the hypothesis that restart-product formation is coupled to the transition from stalled fork to full-length DNA. Additionally, the putative uncoupled product of the CPD-template reaction was composed solely of leading-strand stall products (Fig. 2B), as would be predicted if, in some cases, template unwinding and lagging-strand synthesis continued to the end of the template but leading-strand reinitiation did not occur (*7*, *8*).

To investigate whether restart products were the result of leading-strand synthesis, we exploited the manner in which the Tus-*ter* complex arrests replication by using DNA gyrase to relax positive supercoiling (fig. S7). Under these conditions, the clockwise moving fork is replicated to the Tus-*ter* complex. The leading strand will extend to the first nucleotide of *terB*, whereas the lagging strand terminates 50 to 100 bp upstream, generating a region of ssDNA specifically on the lagging-strand template (*12*). Postreplication Eco RI–Pvu I cleavage should therefore only release leading-strand products as full-length duplex DNA (Fig. 3A). Figure 3B shows that the full-length products of an undamaged-template replication reaction were composed exclusively of leading-strand products. The equivalent result was obtained with the CPD template, in both bulk (Fig. 3C) and column-isolated reactions (fig. S8). However, the full-length duplex products were composed of two nascent chains—the stall and restart—unequivocally showing that restart products were generated by leading-strand synthesis.

To determine if these products were primase dependent, column-isolated, replisome-associated ERIs were released by Eco RI cleavage in the presence or absence of DnaG. In the absence of DnaG, there was virtually no full-length duplex DNA generated (Fig. 4, native). The major reaction product migrated at the position of the uncoupled band and was resistant to Eag I cleavage, demonstrating that it was single stranded beyond the CPD. Consistent with these findings, the denaturing gel revealed that restart-product formation was entirely dependent on DnaG, supporting the finding that DnaG can reinitiate leading-strand synthesis by repriming the leading-strand template (*10*).

Our data show that the *E. coli* replisome can tolerate leading-strand template lesions by remaining associated with the DNA and reinitiating leading-strand synthesis downstream of the damage via DnaG-dependent leading-strand repriming. The reaction is independent of the replication restart proteins, demonstrating that it is an inherent property of the replisome. Bypass of lesions in this manner will generate ssDNA gaps behind the replication fork (*6*) that are predominantly repaired by the faithful process of RecA-dependent recombination (*18*). Because the SOS response will not be induced, this mechanism should be particularly advantageous under normal growth conditions when low levels of damage are present, thereby avoiding cell-division arrest and the induction of mutagenic translesion polymerases. However, the leading-strand reinitiation that we observe is not complete and therefore replisome dissociation may occur, the chances of which will be increased when there are multiple lesions in the template, such as under conditions of replication stress. Should the replisome dissociate, origin-independent replisome loading and SOS-inducible systems such as nuclear excision repair and translesion polymerases are likely to become central to cell survival.

References and Notes

1. H. Merrikh, C. Machón, W. H. Grainger, A. D. Grossman, P. Soultanas, *Nature* **470**, 554 (2011).
2. M. M. Cox *et al.*, *Nature* **404**, 37 (2000).
3. C. P. Guy *et al.*, *Mol. Cell* **36**, 654 (2009).
4. P. McGlynn, R. G. Lloyd, *Nat. Rev. Mol. Cell Biol.* **3**, 859 (2002).
5. W. D. Rupp, P. Howard-Flanders, *J. Mol. Biol.* **31**, 291 (1968).
6. V. N. Iyer, W. D. Rupp, *Biochim. Biophys. Acta* **228**, 117 (1971).
7. K. Higuchi *et al.*, *Genes Cells* **8**, 437 (2003).
8. V. Pagès, R. P. Fuchs, *Science* **300**, 1300 (2003).
9. P. McInerney, M. O'Donnell, *J. Biol. Chem.* **279**, 21543 (2004).
10. R. C. Heller, K. J. Marians, *Nature* **439**, 557 (2006).
11. R. C. Heller, K. J. Marians, *Nat. Rev. Mol. Cell Biol.* **7**, 932 (2006).
12. T. M. Hill, K. J. Marians, *Proc. Natl. Acad. Sci. U.S.A.* **87**, 2481 (1990).
13. H. Hiasa, K. J. Marians, *J. Biol. Chem.* **269**, 16371 (1994).
14. K. J. Marians, H. Hiasa, D. R. Kim, C. S. McHenry, *J. Biol. Chem.* **273**, 2452 (1998).
15. K. M. Carr, J. M. Kaguni, *J. Biol. Chem.* **276**, 44919 (2001).
16. C. A. Wu, E. L. Zechner, K. J. Marians, *J. Biol. Chem.* **267**, 4030 (1992).
17. R. Reyes-Lamothe, D. J. Sherratt, M. C. Leake, *Science* **328**, 498 (2010).
18. A. Berdichevsky, L. Izhar, Z. Livneh, *Mol. Cell* **10**, 917 (2002).

Acknowledgments: We thank S. Bahng for establishing the protocol for replicating M13 DNA primed with the CPD oligonucleotide and C. Gabbai, S. Gupta, and S. Shuman for advice on the manuscript. These studies were supported by NIH grant GM34557.

Supporting Online Material

www.sciencemag.org/cgi/content/full/334/6053/235/DC1
Materials and Methods
Figs. S1 to S8
References

31 May 2011; accepted 1 September 2011
10.1126/science.1209111

Sequential Establishment of Stripe Patterns in an Expanding Cell Population

Chenli Liu,[1]* Xiongfei Fu,[2]* Lizhong Liu,[1] Xiaojing Ren,[3] Carlos K.L. Chau,[1] Sihong Li,[2] Lu Xiang,[1] Hualing Zeng,[2] Guanhua Chen,[3] Lei-Han Tang,[4] Peter Lenz,[5] Xiaodong Cui,[2] Wei Huang,[1,2]† Terence Hwa,[6]† Jian-Dong Huang[1]†

Periodic stripe patterns are ubiquitous in living organisms, yet the underlying developmental processes are complex and difficult to disentangle. We describe a synthetic genetic circuit that couples cell density and motility. This system enabled programmed *Escherichia coli* cells to form periodic stripes of high and low cell densities sequentially and autonomously. Theoretical and experimental analyses reveal that the spatial structure arises from a recurrent aggregation process at the front of the continuously expanding cell population. The number of stripes formed could be tuned by modulating the basal expression of a single gene. The results establish motility control as a simple route to establishing recurrent structures without requiring an extrinsic pacemaker.

Living organisms display an amazing array of regular spatial patterns (*1*–*4*). Traditionally, elucidation of their developmental mechanisms has been pursued through forward or reverse genetics (*3*, *5*). However, essential components required for pattern formation and control are often buried in the overwhelmingly complex physiological context. Synthetic biology provides an engineering approach to examine strategies of pattern formation (*6*–*8*). Recently, efforts have been made to emulate patterning systems with predeposited positional cues (*9*, *10*). These studies do not address spatial or temporal self-organization, which is key to morphogenesis. Indeed, coordinated cell movement in response to self-generated cues is important in embryonic development (*11*–*13*). Here, we investigate striking patterns that emerge in growing bacterial

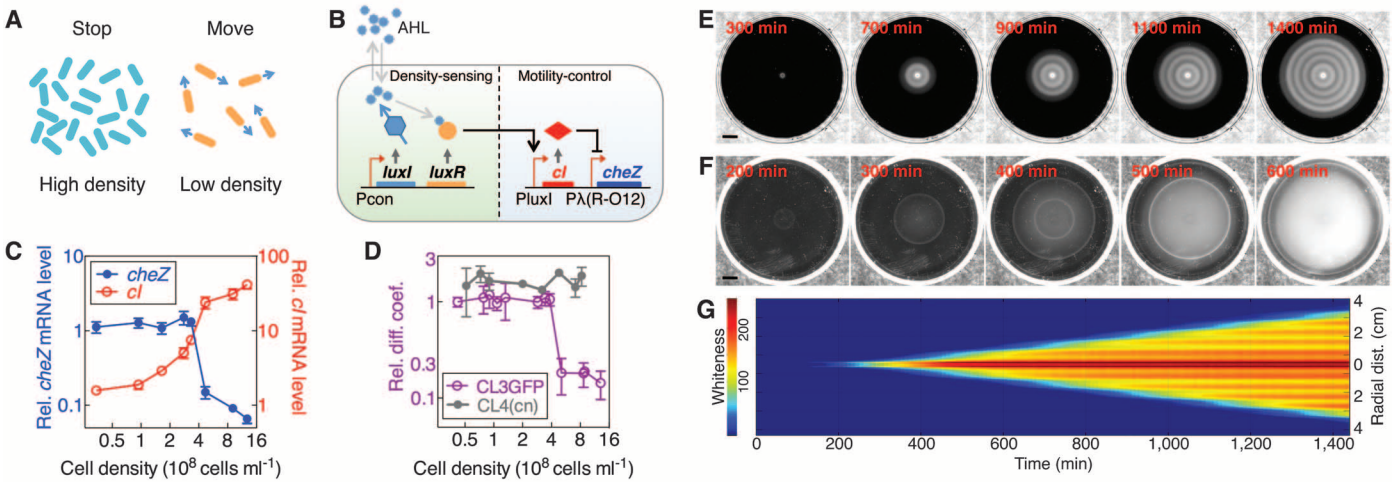

Fig. 1. Spatiotemporal patterns formed by engineered *E. coli* strains. (**A**) Illustration of the desired cell behavior. (**B**) Design of the genetic circuit; see text. (**C**) Relative *cheZ* and *cI* mRNA level in strain CL3 as a function of cell density in bulk culture by qRT-PCR. Data are normalized by the mean value of cells at 0.3×10^8 cells ml^{-1}. (**D**) The relative diffusion coefficient as a function of cell density. CL3GFP, strain CL3 carrying superfolder GFP. CL4(cn), strain CL4 as a control (carrying density-sensing module but with native *cheZ* regulation) (*18*). Relative diffusion coefficient values are normalized by the mean value of CL3GFP at 0.4×10^8 cells ml^{-1}. Results are representative data from three independent experiments. Error bars represent the SD of three replicates. Time-lapsed photographs of typical patterns obtained for the engineered strain CL3 (**E**) and the control strain CL4 (**F**); see also movies S1 and S2. (**G**) Spatiotemporal diagram of (E). All experiments were carried out at 37°C. Scale bars, 1 cm.

populations when cell motility is controlled by cell density, construed as one of the simplest examples of morphogenic cues (*14*).

We constructed a genetic circuit to suppress the motility of *Escherichia coli* cells at high cell densities (Fig. 1A). The circuit is composed of two modules: a density-sensing module and a motility-control module (Fig. 1B). The quorum-sensing system in *Vibrio fischeri* was adopted as the density-sensing module to signal the local cell density. This system synthesizes and excretes a small-molecule acyl-homoserine lactone (AHL), which, at high extracellular concentrations (reflecting high cell density), accumulates intracellularly and activates a constitutively expressed regulator, LuxR (*15*). The motility-control module was devised to modify bacterial motility by regulating the transcription of *cheZ*. *cheZ* deletion causes cells to tumble incessantly, resulting in a nonmotile phenotype in semisolid agar (*16*). Reintroducing *cheZ* restores cell motility (*17*). In our circuit, coupling of the two modules was achieved via the lambda repressor (CI): The LuxR-AHL complex drove the expression of CI that in turn repressed *cheZ* transcription (Fig. 1B). On the basis of this design, we created an engineered strain, CL3 (*18*).

Gene expression of the strain CL3 at various cell densities was quantitatively characterized with quantitative reverse transcription–polymerase chain reaction (qRT-PCR). As designed, *cI* expression level (red) increased more than 40-fold as cell density increased, whereas *cheZ* expression (blue) decreased sharply to 5% of the peak level (Fig. 1C). Cell motility was measured in semisolid agar with a modified continuous fluorescence photobleaching (CPB) method (*18*). It dropped abruptly at a density of ~4×10^8 cells ml^{-1} (Fig. 1D, purple symbols).

When a suspension of exponentially growing CL3 cells was inoculated at the center of a 8.5-cm Petri dish containing 10 ml of LB medium and 0.25% agar, a pattern of alternating white (high cell density) and dark (low cell density) stripes developed overnight (Fig. 1E and movie S1) (*18*). The stripes formed sequentially, at a spacing of ~0.5 cm once every ~2 hours. These stripes were stable for days until the agar completely dried up. As a control, strain CL4 (carrying the density-sensing module but with the native *cheZ* regulation) behaved like the wild type (*16*): From the position of the inoculum, two traveling waves successively moved radially outwards, followed by a uniform expansion of cell density without stripes (Fig. 1F and movie S2). We further verified that each element in the designed genetic circuit is necessary for the stripe

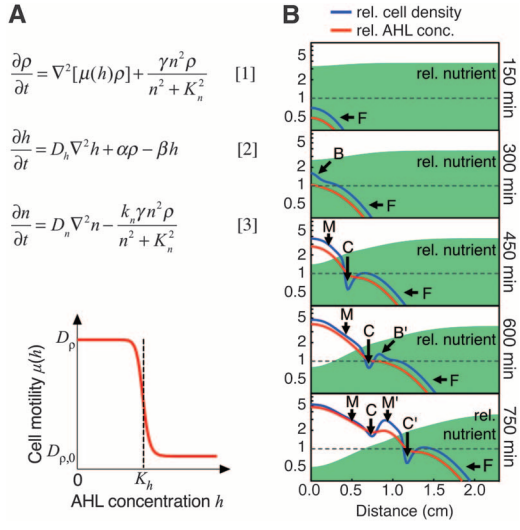

Fig. 2. Kinetic model of autonomous periodic stripe pattern formation. (**A**) The model comprises three key ingredients: cell density (ρ), AHL concentrations (*h*), and nutrient levels (*n*); see text and (*18*). The key feature of this model is that the AHL-dependent cell motility μ(*h*), in light of the data in Fig. 1D, is modeled by a steep Hill function (red line) with an abrupt transition between the values D_ρ and $D_{\rho,0}$ at $h \approx K_h$ (vertical dashed line). (**B**) Time-lapse plots of the simulated relative cell-density profiles ρ(***x***, *t*) (blue), AHL concentrations *h*(***x***, *t*) (red), and nutrient levels *n*(***x***, *t*) (green shade); see also movie S4. The AHL threshold of motility regulation K_h is shown as the horizontal dashed line; the vertical axis is rescaled to cell density (10^8 cells ml^{-1}) (*18*). The periodic pattern is seen as a recurrent process involving the formation of a bud (B); the bud subsequently grows into a stationary mound (M), and a cleft (C) structure forms in a region between the bud and the expanding front (F).

[1]Department of Biochemistry, The University of Hong Kong, Pokfulam, Hong Kong, China. [2]Department of Physics, The University of Hong Kong, Pokfulam, Hong Kong, China. [3]Department of Chemistry, The University of Hong Kong, Pokfulam, Hong Kong, China. [4]Department of Physics, Hong Kong Baptist University, Kowloon Tong, Kowloon, Hong Kong, China. [5]Department of Physics and Center for Synthetic Microbiology, University of Marburg, 35032 Marburg, Germany. [6]Center for Theoretical Biological Physics, University of California at San Diego, La Jolla, CA 92093–0374, USA.

*These authors contributed equally to this work.
†To whom correspondence should be addressed. E-mail: jdhuang@hku.hk (J.D.H.); hwa@ucsd.edu (T.H.); huangwei@hku.hk (W.H.)

pattern formation (fig. S1). We also surveyed the effect of nutrient content, agar thickness, humidity, starting cell number, volume, and growth phase, and found the pattern to be robust to most conditions tested (fig. S2). Notably, the stripe pattern persists even in *cheB*$^-$*cheR*$^-$ double mutants incapable of chemotaxis [fig. S2J (*19*)] but still able to swim and tumble randomly, indicating that the stripes are not a result of chemotactic signaling (*20*). Also, no stripe pattern resulted if CL3 cells were spotted on agar premixed with a low level of CL3 cells in otherwise identical conditions (fig. S2K), indicating that the pattern is not a result of spontaneous amplification of density fluctuations, as would follow from the paradigm of Turing instability (*21*, *22*).

We monitored the spatiotemporal cell density profiles from optical absorbance of the plates [fig. S3 and (*18*)]. Figure 1G displays the time course of light intensities along a diagonal that goes through the inoculum, with the color codes indicating the intensity as in Fig. 1E. It shows that once formed, the pattern of low and high cell densities was frozen in space. Furthermore, new stripes of high cell density emerged at regular time and distance intervals. The same phenomenon was observed in a rectangular geometry when bacterial growth was initiated along a thin line in the middle of the plate (*18*). Stripes developed and propagated toward the opposite edges for CL3 (fig. S4A and movie S3) but not for the wild type or CL4 cells. Fourier analysis revealed high spatial periodicity, with a wavelength of 0.5 cm (fig. S4B).

To gain a quantitative understanding of the patterning process, we developed a mathematical model based on the characterized properties of the engineered circuit (Fig. 2) (*18*). The stochastic swim-and-tumble motion of bacterial cells is described at the population level by a diffusion-like equation (Eq. S1) for the cell density $\rho(\boldsymbol{x}, t)$. The synthesis, diffusion, and turnover of AHL are described by Eq. S2, while the consumption and diffusion of the nutrient $n(\boldsymbol{x}, t)$ are described by Eq. S3. The AHL-dependent motility enters through a phenomenological diffusion coefficient $\mu(h)$ that drops abruptly where the local AHL concentration $h(\boldsymbol{x}, t)$ exceeds a threshold level K_h (Fig. 2A). Numerical simulations of Eqs. S1 to S3 (*23*) with realistic parameter values (table S3) (*18*) generated patterns similar to the experimental observations in both one- and two- dimensional geometries (figs. S5 and S20). The model also captures the more elaborate patterns formed by multiple seeding (fig. S6).

The mathematical model reveals an intriguing sequence of events at the propagating front (Fig. 2B and movie S4). Early on (T = 150 min), cell density (blue line) grows and propagates laterally just as the Fisher wave front (*2*) because the AHL concentration (red line) is uniformly below the threshold level K_h (gray dashed line) due to the low initial cell density. A while later (T = 300 min), the AHL level exceeds the threshold in a region behind the front owing to local cell proliferation: There, a "bud" (marked by B) shoots up in the density profile. Meanwhile, the front (marked by F), which is unaffected by what happens behind because of its low density, continues to propagate laterally at the same speed. Later (T = 450 min), the bud in the density profile grows into a "mound" (marked by M), separated from the frontal region by a "cleft" (marked by C). The continued cell proliferation in the region just behind the front drives up the AHL level and subsequently produces a new bud (B′ at T = 600 min), while the lateral movement of the mound and cleft eventually stops (M and C at T = 600 min). The new bud starts a new stripe of low-motility cells, which again expands into a mound (M′ at T =750 min) delimited by a cleft (C′ at T = 750 min) from the propagating front, and the process repeats itself. Well behind the front, cell proliferation in both the mound and cleft eventually stops as the nutrient is depleted (height of green shade).

The development of a cleft that separates the propagating front from the dense zone of cells behind, and the budding within the frontal region, result from an aggregation phenomenon driven by density-dependent motility discussed in recent theoretical studies (*21*, *24*) and illustrated in Fig. 3A. Cells can diffuse freely in semisolid agar when the cell density is low (top panel). As cells proliferate and the local AHL level exceeds the threshold, cell motility slows down as programmed (middle panel, with the nonmotile cells in teal). These cells cannot move away, but neighboring cells may continue to move into this high-density region and become nonmotile (bottom panel), leading to a net cell flow toward the high-density region.

Wild-type *E. coli* cells may aggregate when grown in specific poor-nutrient media owing to the secretion of potent chemoattractants (*25*). To show that cell aggregation in our system is controlled by the synthetic circuit, we created two strains: the senders (CL6) that synthesize AHL but are nonmotile, and the receivers (CL8), capable of receiving AHL and regulating motility but incapable of AHL synthesis. The receiver cells

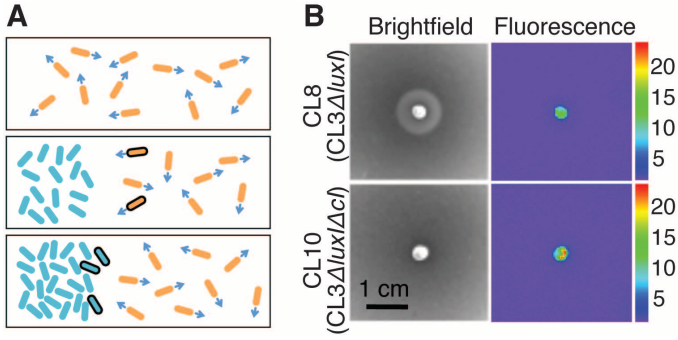

Fig. 3. Cell aggregation driven by density-dependent motility. (**A**) Illustration of aggregation via density-dependent motility; see text. (**B**) Experimental evidence of effective aggregation. Receiver cells were uniformly mixed with 0.25% agar. Five microliters of sender cells (CL6, producing AHL but nonmotile, GFP-expressing) were spotted at the center of receiver-cell–agar mixture, followed by 12-hours' incubation at 37°C. See (*18*) for details. (Upper panels) Strain CL8 (carrying the entire genetic circuit but lacking the AHL-producing gene) as receiver (movie S5). (Lower panels) Strain CL10 (CL8 lacking *cI*) as receiver. (Right panels) Fluorescence photographs indicate the positions of the sender cells.

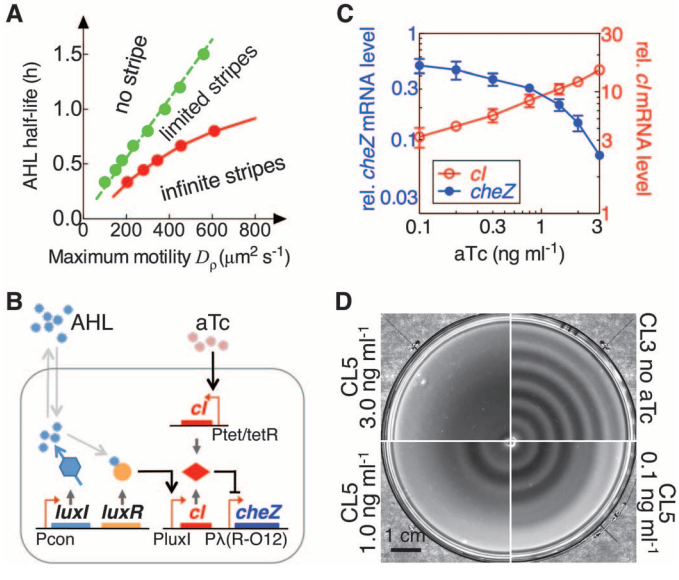

Fig. 4. Tunable stripe patterns. (**A**) Phase diagram; see (*18*, *26*). (**B**) Genetic circuit design for tuning stripe number. An aTc-inducible module was added to vary the expression of *cheZ*. (**C**) Relative *cheZ* and *cI* mRNA level of CL5 in bulk culture containing various concentrations of aTc (0.1 to 3 ng ml^{-1}). Cells were cultured to an absorbance at 600 nm of ~0.05 and harvested for measurement. Data were normalized by the mean value of CL3 at 0.3 × 10^8 cells ml^{-1}. (**D**) Experimental patterns of CL3 (also see fig. S2G) or CL5 inoculated at 0.25% agar containing various concentrations of aTc. Agar plates were incubated at 37°C for 40 hours.

were uniformly mixed with semisolid agar. Subsequently, a drop of sender cells was spotted at the center of the hardened cell-agar mixture. The nonmotile sender cells could not move away from where they were spotted, but were expected to synthesize and excrete AHL as they proliferated at the center of the plate. After a 12-hour incubation, a high-density stripe of receiver cells aggregated around the spotted sender cells (Fig. 3B, upper panels, and movie S5). No aggregation was observed in a control with receiver cells incapable of reducing motility in response to high AHL concentration (CL10) (Fig. 3B, lower panels), or in other controls (fig. S7). Thus, an effective aggregation phenomenon was mediated by density-dependent motility.

Detailed analysis of the mathematical model indicates that the aggregation effect alone is not sufficient to generate stripes. Budding in the frontal region requires the AHL level to exhibit a local maximum, which can happen only when the diffusion length of AHL molecules is sufficiently short (so that the AHL profile closely follows the cell density profile) and the cleft in the cell density profile just behind the front is sufficiently deep. The latter is determined in turn by the parameters, such as the maximum cell motility (*18*, *26*). A key output of the model is summarized by the phase diagram (Fig. 4A), which predicts that in addition to the periodic stripe phase, the engineered strain may exhibit a qualitatively different behavior with no stripes, by passing through a transition region exhibiting a limited number of stripes.

A direct test of the occurrence of the phase transition predicted by the phase diagram (Fig. 4A) is to vary the maximum cell motility (D_ρ in Fig. 2A), thereby changing the number of stripes. Within our experimental design in which motility is set by *cheZ* expression, tuning of D_ρ can be implemented by adding a second *cI* gene, whose expression is titratable in an AHL-independent manner (Fig. 4B). This is implemented in strain CL5 (*18*). Figure 4C shows that the basal *cI* expression level of CL5 cells could indeed be smoothly tuned by adjusting the dosage of an inducer, anhydrotetracycline (aTc), at a fixed cell density (red symbols). Corresponding suppression of *cheZ* expression at low cell density was also observed (blue symbols). For a fixed aTc level, the density dependence of *cheZ* expression remained (fig. S8). When strain CL5 was spotted at the center of semisolid agar, consistent with the model predictions, the number of stripes decreased gradually as the aTc concentration increased from 0.1 to 3.0 ng ml^{-1} (Fig. 4D). As a control, the pattern of strain CL3 did not change even when the aTc concentration was increased to 100 ng ml^{-1} (fig. S2G).

Natural occurrences of well-coordinated spatial and/or temporal patterns are abundant in developmental systems and are believed to involve elaborate control mechanisms (*3*, *5*). Similarly, stripe formation in various bacterial systems (*27*–*29*) has been attributed to complex effects involving chemotaxis, swarming, and differentiation (*4*). Using synthetic circuits, we demonstrate that precise and robust spatiotemporal patterns can be generated autonomously from a very simple interaction—motility control by density. A recurrent mechanism enables structures to form periodically and sequentially. Important features of the pattern such as the number of stripes can be manipulated by tuning components of the circuit, such as the basal expression level of a single gene.

The strategy of sequential stripe formation is likely not limited to cellular motility control. In the kinetic equations S1 to S3 that generated the stripe patterns, the cell density $\rho(\boldsymbol{x}, t)$ is merely an example of a space- and time-dependent variable. Another example could be the concentration of a diffusible molecule, which stimulates its own synthesis to mimic the effect of "cell growth." Thus, Eqs. 1 to 3 may be taken as a generalized reaction-diffusion system with the key feature that the mobility or transport of one of the regulators between adjacent cells is regulated by another mobile regulator. As regulated mobility of signaling molecules is a common strategy in metazoan development (*30*, *31*), the lessons from this work may stimulate new insights and inspire new directions in the studies of developmental systems. For example, the sequential establishment of a periodic somite structure during vertebrate embryonic development is commonly assumed to be controlled by an enabling clock coupled to a sweeping morphogen gradient (*32*). Our results suggest that a spatially periodic structure can be formed autonomously without the need for a clock.

References and Notes

1. L. I. Held, *Models for Embryonic Periodicity* (Karger, Basel, 1992).
2. J. D. Murray, *Mathematical Biology: I. An Introduction* (Springer, New York, ed. 3, 2002).
3. C. M. Chuong, M. K. Richardson, *Int. J. Dev. Biol.* **53**, 653 (2009).
4. E. Ben-Jacob, I. Cohen, H. Levine, *Adv. Phys.* **49**, 395 (2000).
5. E. H. Davidson, D. H. Erwin, *Science* **311**, 796 (2006).
6. A. S. Khalil, J. J. Collins, *Nat. Rev. Genet.* **11**, 367 (2010).
7. M. Elowitz, W. A. Lim, *Nature* **468**, 889 (2010).
8. S. Mukherji, A. van Oudenaarden, *Nat. Rev. Genet.* **10**, 859 (2009).
9. S. Basu, Y. Gerchman, C. H. Collins, F. H. Arnold, R. Weiss, *Nature* **434**, 1130 (2005).
10. M. Isalan, C. Lemerle, L. Serrano, *PLoS Biol.* **3**, e64 (2005).
11. P. Rørth, *Trends Cell Biol.* **17**, 575 (2007).
12. D. J. Montell, *Curr. Opin. Genet. Dev.* **16**, 374 (2006).
13. A. Aman, T. Piotrowski, *Dev. Biol.* **341**, 20 (2010).
14. L. E. Weiss *et al*., *Biotechnol. Bioeng.* **100**, 1251 (2008).
15. C. M. Waters, B. L. Bassler, *Annu. Rev. Cell Dev. Biol.* **21**, 319 (2005).
16. A. J. Wolfe, H. C. Berg, *Proc. Natl. Acad. Sci. U.S.A.* **86**, 6973 (1989).
17. M. G. Sanna, M. I. Simon, *J. Bacteriol.* **178**, 6275 (1996).
18. Materials and methods are available as supporting material on *Science* Online.
19. J. S. Parkinson, S. E. Houts, *J. Bacteriol.* **151**, 106 (1982).
20. H. C. Berg, *Annu. Rev. Biophys. Bioeng.* **4**, 119 (1975).
21. M. E. Cates, D. Marenduzzo, I. Pagonabarraga, J. Tailleur, *Proc. Natl. Acad. Sci. U.S.A.* **107**, 11715 (2010).
22. A. M. Turing, *Philos. Trans. R. Soc. Lond. B Biol. Sci.* **237**, 37 (1952).
23. We believe that Eqs. S1 to S3 comprise the minimalistic, experimentally faithful model needed to generate the observed patterns. A simplified model in which the explicit description of nutrient dynamics was replaced by a growth saturation term (Eq. S11) could initiate but not maintain the patterns, because cell density eventually took on the saturation value everywhere in space (fig. S17A). A related density-only model (*21*) generated stripe patterns by balancing cell aggregation with cell death [see also (*18*)]; it is not applicable to our experiments because cells stop growing but do not die on the relevant time scales. The density-only model also predicted patterns to form from small initial density fluctuation, in contrast to our observation (fig. S18) and model output (*18*).
24. J. Tailleur, M. E. Cates, *Phys. Rev. Lett.* **100**, 218103 (2008).
25. E. O. Budrene, H. C. Berg, *Nature* **349**, 630 (1991).
26. Equations S1 to S3 can produce a variety of stripe patterns depending on the values of two key parameters, maximum motility D_ρ and AHL half-life ln2/β, as summarized in the phase diagram (Fig. 4A); see (*18*) for details. To the right of the solid red line, the system exhibits the periodic stripe phase with an infinite number of stripes. Moving to the left of the solid line, there is a regime where the system can still generate a limited number of stripes for some initial conditions. Far away from the solid line, no stripes can form. The separation between the latter two regimes is not clear-cut and is indicated by the dashed green line. Additional effects such as chemotaxis (Eq. S17) have been investigated. They modify the detailed appearances of the patterns as well as the location of the phase boundaries (fig. S21). The general occurrence of the periodic stripes in this class of models does not require such effects.
27. H. Fujikawa, *Physica A* **189**, 15 (1992).
28. T. Matsuyama *et al*., *J. Bacteriol.* **182**, 385 (2000).
29. D. E. Woodward *et al*., *Biophys. J.* **68**, 2181 (1995).
30. L. Niswander, *Nat. Rev. Genet.* **4**, 133 (2003).
31. M. Affolter, K. Basler, *Nat. Rev. Genet.* **8**, 663 (2007).
32. O. Pourquié, *Science* **301**, 328 (2003).

Acknowledgments: We are grateful to members of the University of Hong Kong Team for The International Genetic Engineering Machine Competition (iGEM) 2008 for their contribution to the project. We thank H. Berg, A. Courey, A. Danchin, D. Smith, J. Tailleur, and C. Voigt for valuable comments. This project was supported by a Hong Kong University (HKU) University Development Fund, a Small Project Grant from the HKU Committee on Research and Conference Grants, and a Collaborative Research Fund from the Research Grants Council (RGC) (HKU1/CRF/10) to J.D.H., and a HKU Faculty of Medicine Development Fund to W.H. TH is supported by the NSF through the Center for Theoretical Biological Physics (grant PHY-0822283) and additionally acknowledges an HKU Distinguished Visiting Professorship. P.L. acknowledges support through the LOEWE program of the State Hessen. L.H.T. acknowledges support by the RGC of the Hong Kong Special Administrative Region under grant 201606. *E. coli* strains and plasmids are available under a material transfer agreement with the University of Hong Kong.

Supporting Online Material

www.sciencemag.org/cgi/content/full/334/6053/238/DC1
Methods
SOM Text
Figs. S1 to S21
Tables S1 to S3
References (*33*–*63*)
Movies S1 to S5

31 May 2011; accepted 2 September 2011
10.1126/science.1209042